

Laven Mavarani\*, Philipp Hillger, Thomas Bücher, Janusz Grzyb, Quentin Cassar, Amel Al-Ibadi, Thomas Zimmer, Gaëtan MacGrogan, Jean-Paul Guillet, Patrick Mounaix and Ullrich R. Pfeiffer

# NearSense – Advances Towards a Silicon-Based Terahertz Near-Field Imaging Sensor for Ex Vivo Breast Tumour Identification

<https://doi.org/10.1515/freq-2018-0016>

Received January 9, 2018

**Abstract:** Breast Cancer is one of the most frequently diagnosed cancer diseases worldwide, and the most common invasive tumour for women. As with all cancers, early detection plays a major role in reducing the mortality and morbidity rate. Currently, most breast cancers are detected due to clinical symptoms, or by screening mammography. The limitations of these techniques have resulted in research of alternative methods for imaging and detecting breast cancer. Apart from this, it is essential to define precise tumour margins during breast-conserving surgeries to reduce the re-excision rate. This study presents the advances in the development of a silicon-based THz sub-wavelength imager usable in life science applications, especially for tumour margin identification.

**Keywords:** tumor margin identification, terahertz waves, medical imaging, near-field sensor, silicon technology

---

\*Corresponding author: **Laven Mavarani**, Institute for High-Frequency, and Communication Technology, University of Wuppertal, 42119 Wuppertal, Germany, E-mail: mavarani@uni-wuppertal.de

**Philipp Hillger:** E-mail: hillger@uni-wuppertal.de, **Thomas Bücher:** E-mail: buecher@uni-wuppertal.de, **Janusz Grzyb:** E-mail: grzyb@uni-wuppertal.de, Institute for High-Frequency, and Communication Technology, University of Wuppertal, 42119 Wuppertal, Germany

**Quentin Cassar:** E-mail: quentin.cassar@ubordeaux.fr,

**Amel Al-Ibadi:** E-mail: amel.al-ibadi@u-bordeaux.fr,

**Thomas Zimmer:** E-mail: thomas.zimmer@ims-bordeaux.fr, University of Bordeaux, IMS UMR CNRS 5218, 33400 Talence, France

**Gaëtan MacGrogan,** Institute Bergonié, Centre Régional de Lutte Contre le Cancer, 229 cours de l'Argonne, 33076 Bordeaux, France, E-mail: G.MacGrogan@bordeaux.unicancer.fr

**Jean-Paul Guillet:** E-mail: jean-paul.guillet@u-bordeaux.fr,

**Patrick Mounaix:** E-mail: patrick.mounaix@u-bordeaux.fr, University of Bordeaux, IMS UMR CNRS 5218, 33400 Talence, France

**Ullrich R. Pfeiffer,** Institute for High-Frequency, and Communication Technology, University of Wuppertal, 42119 Wuppertal, Germany, E-mail: ullrich.pfeiffer@uni-wuppertal.de

## 1 Introduction

Cancer is one of the leading causes of morbidity and mortality worldwide, with approximately 14 million new cases reported in 2012 [1]. The number of new cases per year is expected to rise by about 70% over the next two decades. Breast cancer (*Mamma Carcinoma*; BC) is considered the most common cancer in women. Currently, the average risk of a woman in the United States developing breast cancer sometime in her life is about 12% [2] Countries where industrialization is a more recent phenomenon have a rising incidence and higher mortality [3]. The commonly used screening method is a combination of clinical examination, mammography and ultrasound. These methods provide a good indication whether a lump is cancerous or not. Mammography is one of the most effective detection techniques so far, but it still has a low sensitivity and exposes the patient to ionizing radiation [4]. If a lump is regarded as cancerous, needle biopsies are performed to determine further information about the genetic origin and grade of the cancer. Breast conserving surgeries (also called lumpectomy) are performed to remove the diseased tissue. Removed lymph nodes are examined for remaining tumour cells in the margin tissue. If there are still cancer cells present, a second operation must be performed. Therefore, non-ionizing techniques that offer tumour margin identification with high precision are highly in demand to reduce the re-excision rate [5].

The use of terahertz (THz) technology for life-science applications has recently gained a lot of attention. Frequency dependent absorption lines of liquids and solids have been measured in the past and have shown characteristic spectral fingerprints in the THz region, that make it even possible to gain insights on the bio-molecular level [6, 7]. In the past, studies have demonstrated that THz applications can determine the water, sucrose, alcohol, liquid fuel, and petroleum content [8, 9]. Even collective mode vibrations have been identified for alcohols [10]. Other recent studies have shown that the THz technology makes it possible to quantify the way that

water interacts with biomolecules, which enables the study of molecular hydration [11]. THz is non-ionizing, and can be used without hazards for medical and biological samples [12]. As an example, terahertz time-domain spectroscopy (THz-TDS) has opened many new opportunities in the field of medicine and biology [13]. Studies on breast tumour margins have shown successfully that they are able to distinguish between healthy and diseased tissue [14, 15]. However, the broad utilization of spectroscopic terahertz methods has been held back by the lack of low-cost and compact sensing systems, and the diffraction limitation of terahertz waves for superresolution imaging [16]. In order to overcome the diffraction limit in the THz region, near-field scanning optical microscopy (NSOM) is widely used [17], making it possible to achieve resolutions down to 20–40 nm using atomic force microscopy tips [18]. However, NSOM has the disadvantage of low integration with weak detection signals, or high integration times, and therefore cannot be used for real-time super resolution imaging [19]. On the other hand, THz near-field sensors based on silicon technology have been significantly improved recently, especially when compared to NSOM with regards to sensor sensitivity, system cost, and scanning time [20, 21].

Previously, a silicon-integrated super-resolution near-field sensor with dielectric permittivity-based imaging contrast was presented [20, 21]. The scientific breakthrough is provided by a fully-integrated THz near-field sensor pixel comprising of a THz source (transmitter), an electromagnetic near-field sensor element (transducer), and a THz detector (receiver) including its readout. The THz near-field sensor measures the complex dielectric permittivity, and thereby enables the exploitation of the benefits of terahertz radiation with the required sub-wavelength optical resolution for intraoperative bio imaging. This near-field sensor is based on a commercially available 0.13  $\mu\text{m}$  SiGe-HBT (silicon-germanium heterojunction bipolar transistors) technology and exhibits a lateral resolution that reaches down to 10  $\mu\text{m}$ . Moreover, the architecture of the sensor is compact and scalable, allowing integration of large arrays for scanning time reduction [22]. For this study, the sensor was modified to enable a chopping technique for flicker noise suppression. This results in a highly-improved signal-to-noise-ratio (SNR) that enables the detection of small differences in permittivity, which is a key requirement for the study of medical or biological samples.

In parallel to the development of the near-field sensor, investigations regarding tissue response and imaging contrast of freshly excised breast tissue were performed in the region of 300–600 GHz using THz Time-Domain-Spectroscopy (TDS). These studies demonstrate

that this frequency range provides sufficient contrast between healthy and malignant breast tissues and is well-suited to be used in a fully integrated near-field imaging sensor. In addition, the resolution in near-field measurements provides a resolution closer to the typical eukaryote cell diameter, in contrast to the resolution of regular THz TDS, and thus might enable better discrimination between margins. The knowledge of these frequencies, combined with single-pixel near-field sensors, could be used for the development of a multi-pixel near-field imager for life-science applications [23].

## 2 Experimental setup and results

The present study is divided into two parts: The first part investigates the performance of THz radiation in the 300–600 GHz range to evaluate the potential of spectral terahertz imaging to discriminate healthy from malignant breast tissues. In the second part advances in creating a fully-integrated 0.53 THz near-field sensor, implemented in 0.13  $\mu\text{m}$  SiGe HBT technology for the detection of small changes in dielectric permittivity based contrast, are shown.

### 2.1 THz TDS

A THz TDS spectroscopy system was implemented by the University of Bordeaux directly at the hospital (Institut Bergonié). There, 17 freshly excised breast tissues with different cancer types and grades have been collected, measured, and analyzed just after the excision in the operating room. Complementary, automatic signal and data processing has been developed, based on different statistical methods to explore their feasibility to provide the optimum contrast between benign and malignant breast tissues [23], whilst helping with the low data display complexity level required to transfer such a technique to a hospital.

In Figure 1 two exemplary BC tissue samples are shown. Each of the two samples has been measured at different frequencies between 310–630 GHz in order to determine the frequency associated with the highest resolution and contrast. The images show that the higher frequencies between 490–630 GHz reflect the best resolution, when compared to the tissue structures.

In Figure 2 the same BC tissue sample as in Figure 1 (upper row) is depicted. This time the sample has been measured with THz TDS at 300, 400, 500 and 600 GHz, respectively. On the left side the H&E (Hematoxylin &

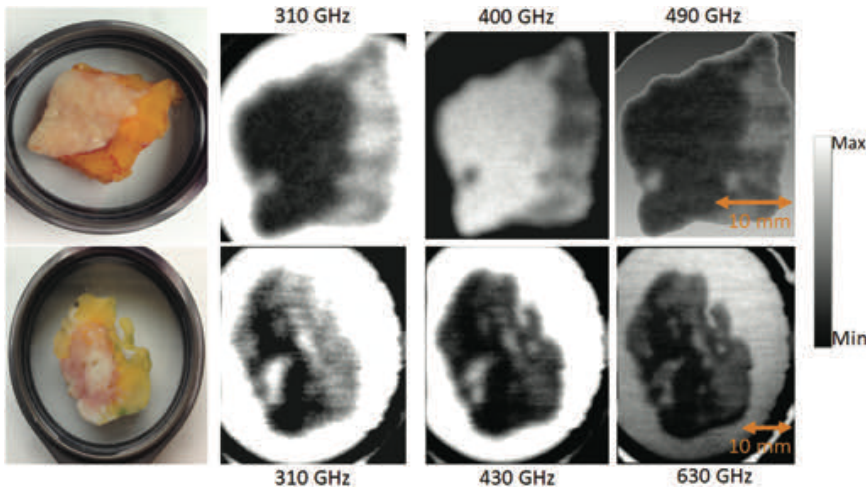


Figure 1: THz-images of BC tissue sections from 310-630 GHz. Higher frequencies show a better resolution in the THz-image compared to the tissue structures measured.

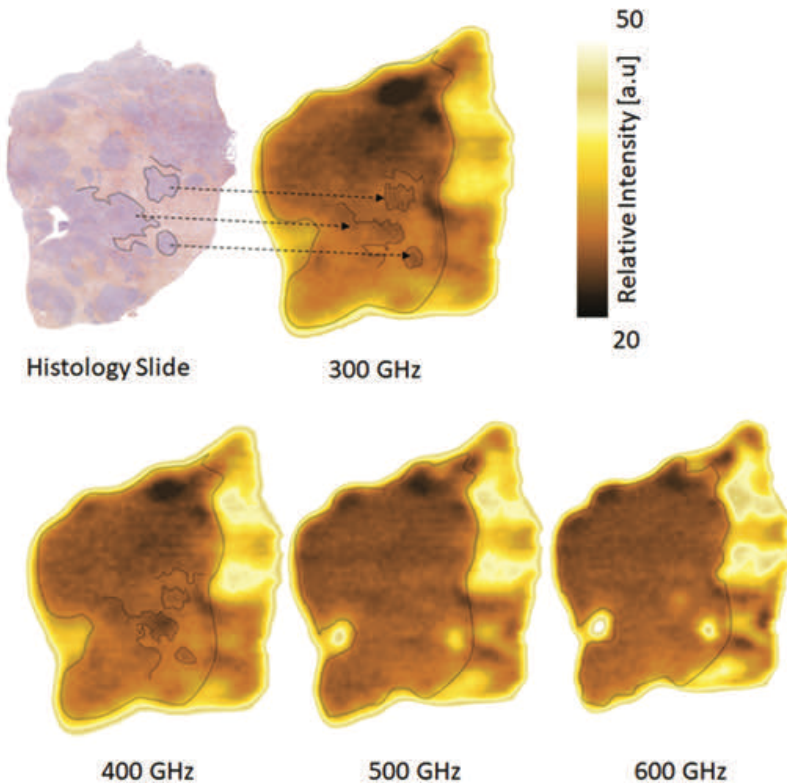


Figure 2: Comparison between the H&E stained histology section of a malignant breast tissue (upper row left) and the corresponding THz-images of same tissue section before deparaffinization at 300, 400, 500 and 600 GHz, respectively (from left to right). The color bar reflects the relative intensities of the THz images.

Eosin) stained histology section of the breast cancer tissue is shown. The adipose tissue is washed out during paraffinization process, and hence is not apparent in the histology slide. The THz-images here relate the reflected signal amplitude in dependence of the refractive index. Features of interest are highlighted with dashed lines

within the tissue and can be compared with the THz TDS images. Frequencies ranging from 300 to 400 GHz exhibit interesting demarcations between cancerous and healthy regions. However, all malignant sectors are not well delineated. For frequencies higher than 600 GHz the contrast is lower, and discrimination is tedious. The contrast loss

for a specific tissue location over the selected working frequency band is mostly induced by the decrease of the signal-to-noise-ratio (SNR) in THz TDS when going to high frequencies [24].

PCA and usual signal processing have been performed, and the results show that the provided differences regarding the reflective index between BC and normal tissue in the region from 300–600 GHz are similar. The differences are small, but sufficient for discrimination of different tissue types when combined with the higher resolution between 500–600 GHz, and may therefore help for intraoperative breast tumour margin detection. These insights open the way for a silicon-based terahertz sub-wavelength imager design, efficient up to 600 GHz to address ex vivo life science applications [24].

## 2.2 Near-field THz sensor

In this present work, a modified version of the fully-integrated near-field single ended sensor pixel previously presented in [21] is shown. This solid-state super-resolution imaging device in 0.13  $\mu\text{m}$  SiGe-HBT technology operates around 534–562 GHz and is fully integrated with a complete imaging functionality, including a tunable continuous wave (CW) illumination source, near-field sensing, and power detection. The heart of the device is a cross-bridged double split-ring resonator (SRR) that features a 3-D topography to achieve high-spatial confinement of the surface near-fields, and is capable of resolving structural details with an estimated lateral resolution down to 10–12  $\mu\text{m}$ . Moreover, the modified sensor pixel device enables chopping of the 0.55 THz oscillator for detector flicker noise suppression. Figure 3 shows the micrograph of the near-field sensor used in this work.

In on-wafer SNR measurements the sensor SNR, defined by the maximum current response to a metallic object divided by the spot-noise, reaches up to 115 dB at a chopping frequency of 25 kHz, being significantly higher than the previously reported 42 dB SNR for the DC-operated sensor (Figure 3). In this way, the sensor can detect even small differences in the permittivity, and thus is capable of a better contrast generation in biological samples.

The first experiments were performed to show that this single ended near-field sensor pixel is capable of imaging. For this purpose, a commercially available STM (Scanning Tunneling Microscope) setup (*Semilab Navigator 220*) was modified, which allows the sensor to be scanned along an object (Figure 4). Therefore, the

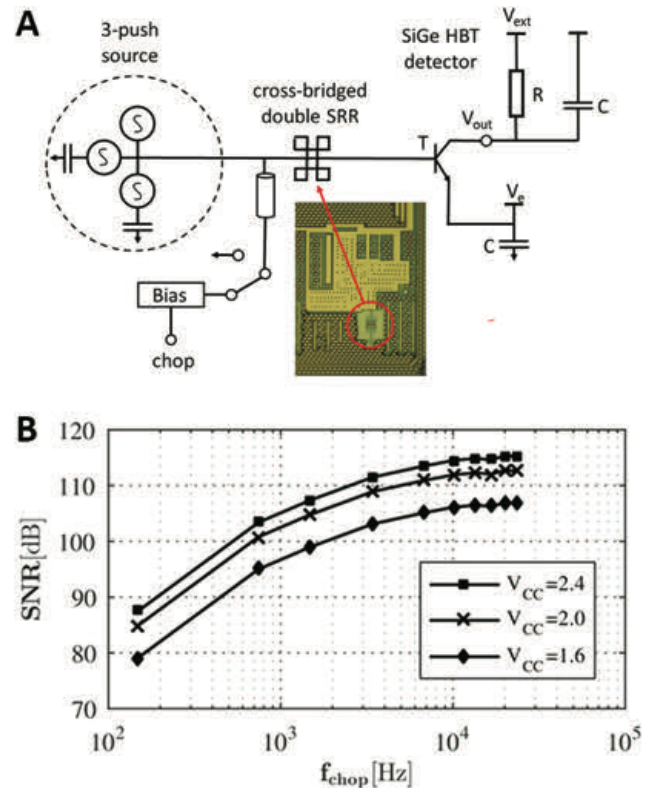


**Figure 3:** A: Simplified schematic and micrograph of the near-field single-ended sensor with the cross-bridged double split-ring resonator (SRR) and chopping. B: SNR measurement of the sensor defined by the maximum current response to a metallic object divided by the spot-noise at the chopping frequency.

sensor is mounted on a z-moveable holder. Using a high-resolution digital CCD camera from below, the sensor is monitored manually for planarization. The sample of interest is subsequently fixed on a holder mounted on a high precision x,y piezo table. For these measurements, the sensor output current was detected with a chopping frequency of 30 kHz.

Imaging results are shown in Figure 5, where the single pixel near-field imager was kept in close proximity to a nickel- (Ni-) mesh without making contact. The measured mesh has a 50  $\mu\text{m}$  bar width and a 250  $\mu\text{m}$  bar pitch (*Veco Specimen Grid 0100-NI*). The 2D image was acquired during a x,y-scan over an area of 60×1000  $\mu\text{m}$  with a step-size of 1 pixel per 10  $\mu\text{m}$ . The scanning time per pixel was set at 8 seconds. The false colour image reflects the structure of the inner mesh. In another measurement, a 200×200  $\mu\text{m}$  scan of a single bar was imaged more precisely. Here, the resolution was selected to 20×20 pixel with a scanning time of 10 seconds per pixel. The thickness of the bar according to the false colour image lies at around 60  $\mu\text{m}$ , which is slightly larger than the actual bar size of the

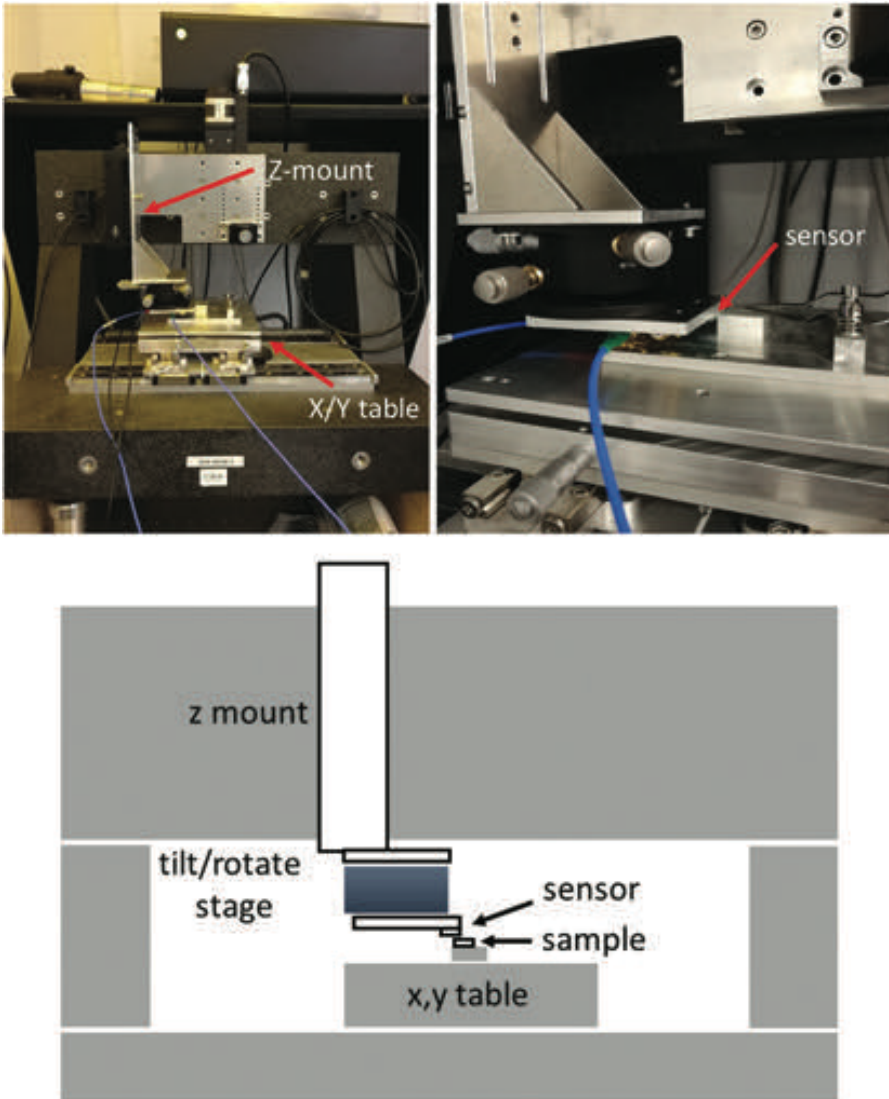


**Figure 4:** Modified STM set-up for near-field sensor scanning experiments. Lower part: Schematic of the set-up showing the sensor attached to a z mount and the sample fixed on a x,y table.

mesh, and a result of the chosen step-size of 1 pixel per  $10\ \mu\text{m}$ . Since these are the results of the first experiments using the described scanning microscope set-up, neither the chosen step-size, nor the scanning time per pixel are optimized. As such, there is still considerable additional scope for the further improvements regarding the set-up and measurement parameters.

### 3 Discussion and conclusion

The set-up using a reflection geometry spectro-THz-imaging system at the Department of Pathology of the Bergoniè Institute has resulted in the measurement

of seventeen freshly excised breast tissue samples of different cancer types and grades. The analysed results indicate that THz-imaging in the area from 300–600 GHz holds significant potential for the discrimination of fatty tissue from the cancer–fibre matrix, and- more important- also shows differences between cancer and normal tissue. Various data and signal processing techniques have also been utilized to enhance the contrast between tissue kinds from raw frequency data. Statistical approaches, such as FD (frequency domain) FWHM (full-width half maximum) and TD (time domain) mean pixel signal over the frequency band, have yielded promising results, bringing additional information on tissue constitution [24]. For more in-depth investigations further tissue samples

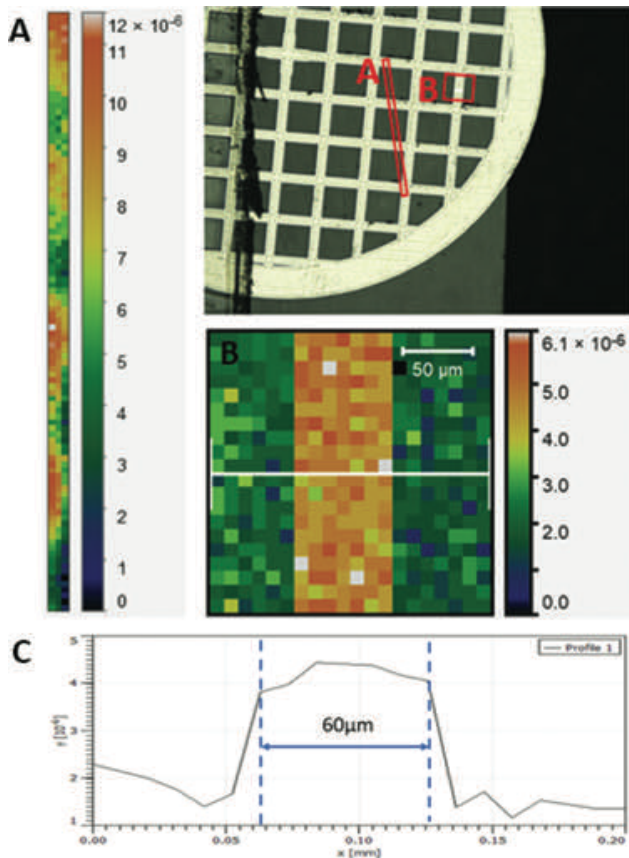


**Figure 5:** False colour imaging using the single pixel near-field imager for a Ni-mesh *Veco Specimen Grid 0100-NI*. The location of image A and B are indicated in the microscopic image of the grid. A: 60x1000  $\mu\text{m}$ , 3x100 px, time/px=8 s; B: 200x200  $\mu\text{m}$ , 20x20 px, time/px=10 s; C: Cross section through the grid bar in B indicated by a white line.

must be measured and analysed. However, the distinction between fibres and cancerous regions has to be improved, but is challenging due to the fast degradation of fresh tissue samples, the low number of available tissue samples, and the poor resolution of THz TDS in the 300–600 GHz range. To overcome these resolution limitation, the near-field sensor described in this study constitutes a promising option, especially in the frequency range from 500–600 GHz. The approach detailed here makes use of advanced silicon process technologies, and may provide the required technology to enable marker-free intraoperative tumour margin identification with terahertz waves. Thereby, the initial challenges were to develop a compact sensor with the appropriate sensitivity and a well-defined sensing area. Since the source, sensor and detector are located in the same plane, the entire circuitry is located under the chip top surface. In this way, the sample-sensor interaction that happens at the chip top surface is not effected by the circuitry. In [20] we successfully realized a sensor device with these properties. The presented

single-ended near-field sensor has further confirmed that a fully integrated single-ended near-field sensor pixel is suited for imaging applications. In a scanning microscope set-up, it was possible to show a scanned false colour image of various areas of a Ni-Mesh using the dielectric permittivity differences between areas of the mesh and areas of the glass plane below it. Although the bars of the mesh were successfully imaged, the extracted width differs from the true value of 50  $\mu\text{m}$  due to the selected step-size. Instead, the results reveal a bar width of 60  $\mu\text{m}$ . To improve the near-field sensor imaging, the scan procedure must be optimized regarding scanning time, which can be significantly reduced up to few milliseconds, and step-size, which is not yet adapted to the possible limit to achieve the best resolution. Scanning time reduction can additionally be addressed by taking advantage of the scalable circuit architecture for array implementation [22]. The major challenges that remain are to identify the relevant bio imaging parameters for tumour margin identification in tissue sample tests. The microscope set-up will be used for future scans of deparaffinized tissue sections, to build up a data base of the relevant differences between the tissue components. A problem remains to be solved: The sensor device needs to be contacted from the backside to enable free movement over large areas. This can be achieved by Silicon-Through-VIAs [25]. The results shown here are a further step towards the goals of the NearSense project, which will open up many new fields of near-field THz imaging in life science applications in future, but especially aims at the use of this sensor device in hospitals on freshly excised samples, which in a next step can be compared to the measurements performed with the THz TDS set-up.

**Funding:** This work is part of the project *NearSense- A silicon-based terahertz near-field imaging array for ex vivo life-science applications* and was funded in the frame of the DFG priority program SPP 1857 *ESSENCE (Elektromagnetic Sensors for Life Sciences)*.

## References

- [1] J. Ferlay, I. Soerjomataram, R. Dikshit, S. Eser, C. Mathers, M. Rebelo, D. M. Parkin, D. Forman, and F. Bray, “Cancer incidence and mortality worldwide: Sources, methods and major patterns in globocan 2012,” *Int. J. Cancer*, vol. 136, no. 5, pp. E359–E386, 2015.
- [2] R. A. Smith, K. S. Andrews, D. Brooks, S. A. Fedewa, D. Manassaram-Baptiste, D. Saslow, O. W. Brawley, and R. C. Wender. Cancer screening in the united states, 2017: a review of current american cancer society guidelines and current

- issues in cancer screening. *CA: A Cancer J. Clinicians*, vol. 67, no. 2, pp. 100–121, 2017.
- [3] B. W. Stewart and C. P. Wild. *World Cancer Report 2014*. International Agency for Research on Cancer. International Agency for Research on Cancer, 2014.
- [4] F. Shtern. Digital mammography and related technologies: a perspective from the national cancer institute. *Radiology*, vol. 183, no. 3, pp. 629–630, 1992.
- [5] S. E. Singletary. Breast cancer surgery for the 21st century: the continuing evolution of minimally invasive treatments. *Minerva Chirurgica*, vol. 61, no. 4, pp. 333–352, 2006.
- [6] X. Yang, X. Zhao, K. Yang, Y. Liu, Y. Liu, W. Fu, and Y. Luo. Biomedical applications of terahertz spectroscopy and imaging. *Trends Biotechnol.*, vol. 34, no. 10, pp. 810–824, 2016.
- [7] N. Karpowicz, H. Zhong, C. Zhang, K.-I. Lin, J.-S. Hwang, J. Xu, and X.-C. Zhang. Compact continuous-wave subterahertz system for inspection applications. *Appl. Phys. Lett.*, vol. 86, no. 5, p. 054105, 2005.
- [8] P. U. Jepsen, U. Møller, and H. Merbold. Investigation of aqueous alcohol and sugar solutions with reflection terahertz time-domain spectroscopy. *Opt. Exp.*, vol. 15, no. 22, pp. 14717–14737, 2007.
- [9] Y.-S. Jin, G.-J. Kim, C.-H. Shon, S.-G. Jeon, and J.-I. Kim. Analysis of petroleum products and their mixtures by using terahertz time domain spectroscopy. *Journal of the Korean Physical Society*, vol. 53, no. 4, pp. 1879–1885, 2008.
- [10] Y. Yomogida, Y. Sato, R. Nozaki, T. Mishina, and J. Nakahara. Comparative dielectric study of monohydric alcohols with terahertz time-domain spectroscopy. *Journal of Molecular Structure*, vol. 981, no. 1, pp. 173–178, 2010.
- [11] V. Conti Nibali and M. Havenith. New insights into the role of water in biological function: Studying solvated biomolecules using terahertz absorption spectroscopy in conjunction with molecular dynamics simulations. *J. Am. Chem. Soc.*, vol. 136, no. 37, pp. 12800–12807, 2014.
- [12] H. H. Mantsch and D. Naumann. Terahertz spectroscopy: The renaissance of far infrared spectroscopy. *J. Mol. Struct.*, vol. 964, no. 1, pp. 1–4, 2010.
- [13] P. H. Siegel. Terahertz technology in biology and medicine. *IEEE Trans. Microwave Theory Tech.*, vol. 52, no. 10, pp. 2438–2447, 2004.
- [14] A. J. Fitzgerald, V. P. Wallace, M. Jimenez-Linan, L. Bobrow, R. J. Pye, A. D. Purushotham, and D. D. Arnone. Terahertz pulsed imaging of human breast tumors. *Radiology*, vol. 239, no. 2, pp. 533–540, 2006.
- [15] A. J. Fitzgerald, S. Pinder, A. D. Purushotham, P. O’Kelly, P. C. Ashworth, and V. P. Wallace. Classification of terahertz-pulsed imaging data from excised breast tissue. *Journal of biomedical optics*, vol. 17, no. 1, pp. 0160051–01600510, 2012.
- [16] X. Hao, C. Kuang, Z. Gu, Y. Wang, S. Li, Y. Ku, Y. Li, J. Ge, and X. Liu. From microscopy to nanoscopy via visible light. *Light Sci. Appl.*, vol. 2, no. 10, p. e108, 2013.
- [17] A. J. L. Adam. Review of near-field terahertz measurement methods and their applications. *J. Infrared Millimeter Terahertz Waves*, vol. 32, no. 8-9, p. 976, 2011.
- [18] H.-T. Chen, R. Kersting, and G. Cho. Terahertz imaging with nanometer resolution. *Appl. Phys. Lett.*, vol. 83, no. 15, pp. 3009–3011, 2003.
- [19] J.-P. Guillet, L. Chusseau, R. Adam, T. Grosjean, A. Penarier, F. Baida, and D. Charrat. Continuous-wave scanning terahertz near-field microscope. *Microwave Opt. Technol. Lett.*, vol. 53, no. 3, pp. 580–582, 2011.
- [20] J. Grzyb, B. Heinemann, and U. R. Pfeiffer. A 0.55 thz near-field sensor with a  $\mu\text{m}$ -range lateral resolution fully integrated in 130 nm sige bicmos. *IEEE J. Solid-State Circuits*, vol. 51, no. 12, pp. 3063–3077, 2016.
- [21] J. Grzyb, B. Heinemann, and U. R. Pfeiffer. Solid-state terahertz superresolution imaging device in 130-nm sige bicmos technology. *IEEE Trans. Microwave Theory Tech.*, 2017.
- [22] P. Hillger, R. Jain, J. Grzyb, L. Mavarani, B. Heinemann, G. Mac Grogan, P. Mounaix, T. Zimmer, and U. Pfeiffer. A 128-pixel 0.56thz sensing array for real-time near-field imaging in 0.13  $\mu\text{m}$  sige bicmos. *IEEE International Solid-State Circuits Conference ISSCC*, pp. 418 - 419, 2018.
- [23] H. Balacey, B. Recur, J.-B. Perraud, J. B. Sleiman, J.-P. Guillet, and P. Mounaix. Advanced processing sequence for 3-d thz imaging. *IEEE Trans. Terahertz Sci. Technol.*, vol. 6, no. 2, pp. 191–198, 2016.
- [24] Q. Cassar, A. Al-Ibadi, L. Mavarani, P. Hillger, J. Grzyb, G. MacGrogan, T. Zimmer, U. R Pfeiffer, J.-P. Guillet, and Mounaix. Contrast analysis of freshly excised malignant and healthy breast tissues in the 300 – 600 ghz range. *To be published*.
- [25] J. U Knickerbocker, C. S. Patel, P. S. Andry, C. K. Tsang, L. P. Buchwalter, E. J. Sprogis, H. Gan, R. R. Horton, R. J. Polastre, S. L. Wright, et al. 3-d silicon integration and silicon packaging technology using silicon through-vias. *IEEE J. Solid-State Circuits*, vol. 41, no. 8, pp. 1718–1725, 2006.